

Multiple-interface coupling effects in local electron-energy-loss measurements of band gap energies

M. Couillard,^{1,2,*} M. Kociak,¹ O. Stéphan,¹ G. A. Botton,² and C. Colliex¹¹Laboratoire de Physique des Solides, CNRS, UMR8502, Université Paris-Sud, 91405 Orsay, France²Department of Materials Science and Engineering, Brockhouse Institute for Materials Research, McMaster University, Hamilton, Canada L8S 4M1

(Received 5 September 2007; published 29 October 2007)

Electron-energy-loss spectroscopy acquired with a subnanometer probe is used to record electron excitation spectra in a nanometer-scale layered structure. When applied to measure band gap energies in a HfO₂ layer, we demonstrate that the desired local information is obscured by delocalized contributions from interface plasmons, interband transitions, and Čerenkov radiation. Simulations performed within a relativistic dielectric formalism, incorporating electromagnetic interaction between all layers in the investigated nanostructure, prove to be essential in identifying the various energy-loss signals, in particular, those associated with multiple-boundary effects.

DOI: 10.1103/PhysRevB.76.165131

PACS number(s): 73.20.Mf, 73.40.Qv, 78.20.Bh, 79.20.Uv

I. INTRODUCTION

Probing dielectric and optical properties with electrons offers the opportunity to exploit the high spatial resolution available in scanning transmission electron microscopes (STEMs). Despite an energy resolution lower than that offered by optical techniques, electron energy-loss spectroscopy (EELS) allows for the dielectric response measurement of individual nanostructures,^{1–5} interfaces,^{6,7} and defects.^{8–10} Recently, for instance, optical gaps of single boron nitride nanotubes have been extracted using EELS.² In order to further explore the potential of this approach, we have investigated the case of a gate stack incorporating a thin layer of HfO₂. This material constitutes a potential candidate to replace SiO₂ as the main dielectric material in metal-oxide-semiconductor devices,¹¹ and it has been the focus of several EELS studies,^{12–16} some of them having used low-loss spectroscopy.^{17,18} In this work, we show that the system, incorporating all the layers and their interfaces, responds as a whole to the Coulomb field induced by incident electrons traveling in one of the layers. In addition to metalliclike interface plasmons, delocalized excitations of interband transitions and radiative modes are also involved in this response. Thus, each layer cannot be investigated independently, thereby preventing straightforward spatially resolved gap measurements.

Electromagnetic field coupling between the electron probe and the sample may generate energy-loss signals associated with the excitation of modes spatially located relatively far from the incident electron trajectory. In particular, interface plasmons (IPs) arising from boundary conditions can be generated by fast electrons traveling few nanometers away from an interface.^{6,19,20} In the nonrelativistic formalism for a flat interface between materials A and B, with dielectric constants ϵ_A and ϵ_B , these contributions are proportional to $\text{Im}[(\epsilon_A - \epsilon_B)/(\epsilon_A + \epsilon_B)]$. Strong IPs are expected when $\text{Re}(\epsilon_A + \epsilon_B) = 0$, and may produce loss signals below the band gap energy of insulators. For a bounded layer, IP coupling becomes significant when the thickness of this layer is on the order of v/ω , where v is the speed of incident electrons and

$\hbar\omega$ is the energy of the interface mode. If the system consists of several layers, then loss spectra should therefore depend on the interaction between all interface modes as well as on the trajectory of the incident electrons.

II. EXPERIMENTS AND SIMULATIONS

The present experiments have been performed on a stack of three layers embedded between two semi-infinite Si media, as represented schematically in Fig. 1(a). From high-resolution transmission electron microscope (TEM) images [Fig. 1(b)], the thicknesses of the layers of SiO₂, HfO₂, and TiN were evaluated as 7.5, 4.0, and 6.5 nm, respectively. Although the width of the SiO₂ layer is thicker than required in real applications, this particular sample offers an ideal opportunity to study IP coupling, because each interface is clearly separated. The sequence of EELS spectra, shown in Fig. 2, has been recorded using the Orsay VG HB501 STEM in the spectrum-image mode²² with an ~ 5 Å diameter electron probe, an acquisition time of 20 ms per spectrum, and a step size of 3 Å. The line scan was acquired at a high specimen thickness of ~ 110 nm (measured with the EELS approach described in Ref. 23) in order to reduce contributions from the two interfaces between the specimen and the

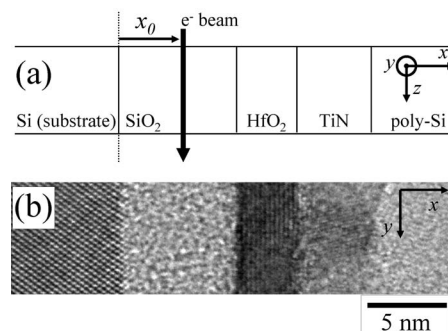


FIG. 1. (a) Schematic view and (b) high-resolution TEM image of the layered system.

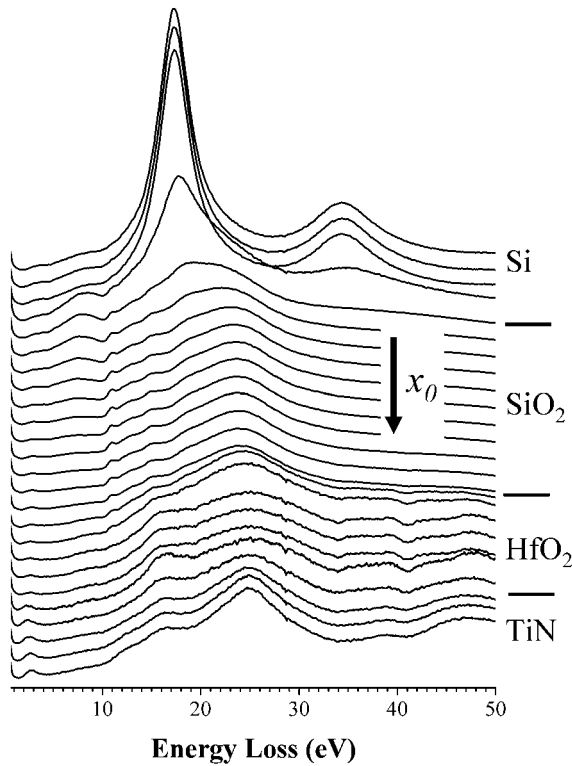


FIG. 2. EELS line scan across the stack from the Si substrate (top) to the TiN layer (bottom). For clarity, only a subset of the original line scan is displayed.

vacuum. The convergence and collection semiangles were 8.4 and 4.4 mrad, corresponding to an effective collection angle²³ of 7.8 mrad that was used in the simulations. Several scans acquired across the stack were aligned spatially and energetically before summing individual spectra to obtain a depth profile. Each spectrum was scaled with respect to its zero loss peak (ZLP) maximum, and then deconvoluted using a maximum likelihood algorithm²⁴ with five iterations in order to improve the visibility of features at low energies. For experimental spectra shown in Figs. 4 and 5, a self-deconvoluted ZLP acquired in vacuum was fitted to and then subtracted from the spectra.

For data interpretation, we use a relativistic model of loss spectra in a stratified system composed of any number of layers, which was derived within the framework of the local dielectric theory by Bolton and Chen.^{20,21} The authors developed a transfer matrix recurrence relation to account for all boundary conditions. For the simulations presented here, complex dielectric constants for Si, SiO₂, and TiN were taken from optical data tabulated in Ref. 25 and those for HfO₂ were extracted from a Kramers-Kronig analysis²³ of EELS spectra recorded on a bulk HfO₂ sample (presented in the next section). We define the coordinates as shown in Fig. 1; the electrons travel along the z direction at a distance x_0 from the nearest interface to the left. The model neglects the convergence angle of incident electrons and assumes an infinite thickness along z .

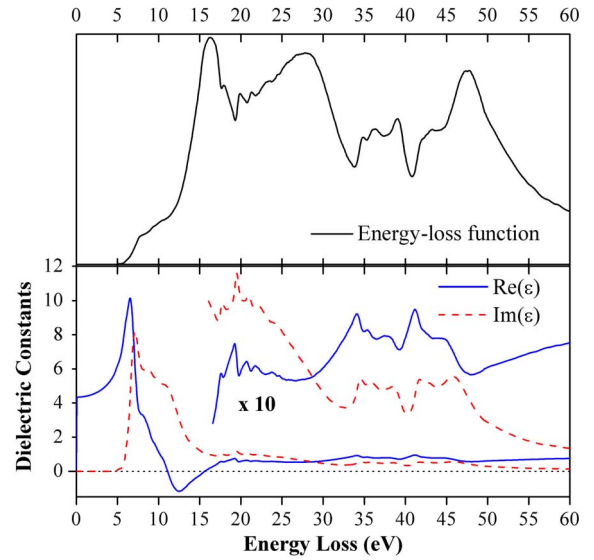


FIG. 3. (Color online) Energy-loss function (top) and complex dielectric constants (bottom) extracted from a Kramers-Kronig analysis of a bulk HfO₂ spectrum.

III. RESULTS AND DISCUSSION

A. Bulk HfO₂

We first describe the prominent structures visible in an EELS spectrum of bulk HfO₂. The EELS analysis was performed on a HfO₂ powder (Sigma-Aldrich Product No. 203394). To avoid beam damage, the electron probe was scanned over uniformly thick area to collect several spectra (~ 200 spectra, with an individual acquisition time of 50 ms). These spectra were aligned in energy and summed. A Kramers-Kronig analysis²³ was then performed on single-scattering distributions obtained from the spectra using routines available in the DigitalMicrograph environment. Extensions to the spectra for energy loss up to 200 eV ensured an accurate energy integration. Corrections to take into account the collection angle and the surface contributions were also included. Finally, the dielectric function was normalized using the optical refractive index of HfO₂ [$n=2.1$ (Ref. 26)].

Figure 3 presents the energy-loss function [$\text{Im}(1/\epsilon)$] along with the complex dielectric constants extracted from the Kramers-Kronig analysis. The band gap onset is measured at 5.9 eV, close to the value of 5.8 eV previously cited for monoclinic HfO₂.¹¹ The most intense feature in this spectrum is the bulk plasmon at 16 eV. This plasmon peak is located slightly above the energy where the real part of the dielectric constant crosses zero. It is followed by a series of high-energy interband transitions between 17 and 25 eV, some of them involving oxygen $2s$ electrons. A broad feature around 28 eV is interpreted in terms of a collective excitation, analogous to a similar feature previously observed and analyzed in ZrO₂.²⁷ This energy corresponds to a local minimum in $\text{Re}(\epsilon)$ and has no associated peak in $\text{Im}(\epsilon)$. Finally, the semicore Hf $O_{2,3}$ edges are located above 33 eV.

B. HfO₂ gate stack

When the probe is located at the center of the HfO₂ layer in the stack (curves D in Fig. 4), most of the features iden-

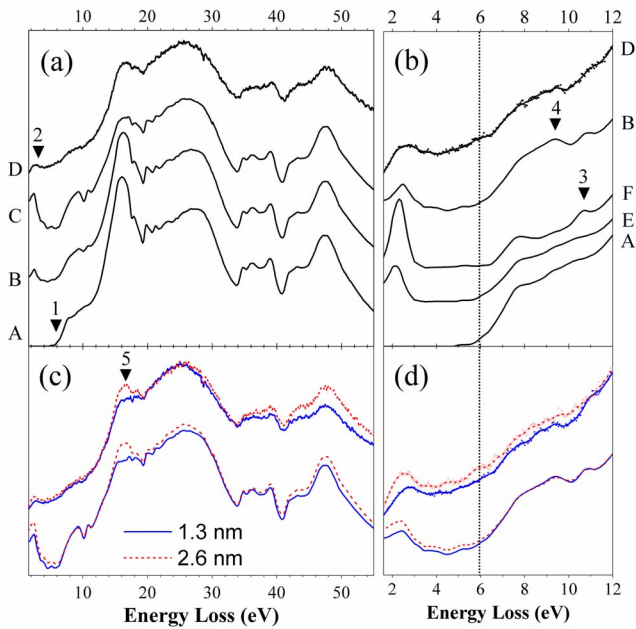


FIG. 4. (Color online) [(a) and (b)] A bulk HfO₂ spectrum (A) and a spectrum acquired in the center of the HfO₂ layer (D) compared with simulation results for various systems (see text). [(c) and (d)] Experimental (top) and modeled (bottom) spectra in the HfO₂ layer for two impact parameters. The values of 1.3 and 2.6 nm refer to an origin at the SiO₂/HfO₂ boundary. A finite thickness correction was included for the modeled spectra in (c). The vertical dotted line indicates the HfO₂ gap onset.

tified in the reference spectrum of bulk HfO₂ (A) can be recognized. However, the gap region below 5.9 eV (arrow 1) contains extra contributions (arrow 2), while changes are also observed at higher energies. Figure 4(b) presents a close-up view of the experimental spectra along with simulated spectra for various configurations. If only the HfO₂/TiN interface is included in the model (E), the simulation clearly predicts the existence of an IP at ~2.5 eV within the HfO₂ gap (5.9 eV, vertical dotted line). For the more complex SiO₂/HfO₂/TiN model (F), the shape of the spectrum both below and above the gap onset is substantially modified. Finally, simulations including all layers produce a spectrum (B) very similar to the experimental one, displaying, for instance, a characteristic dip around 10 eV.

Although the agreement at low energies is good, the discussion leading to the spectrum B fails to explain the changes observed at higher energies [Fig. 4(a)]. The model of Ref. 20 was developed within the local approximation. However, due to the small layer thickness, nonlocal dispersive effects²⁸ could play a role. As a first correction, we follow Ref. 29 and impose on the bulk part of the simulation a lower limit equal to the inverse of the slab thickness for the momentum transferred in the *x* direction. In addition, we set an upper limit corresponding to the EELS aperture. This approximation increases the fraction of signal from interface modes and generates a spectrum (C) that is in better agreement with the experiment (D). We note that the overestimation in the simulated signal at low energies clearly points to a limit in the accuracy of this correction.

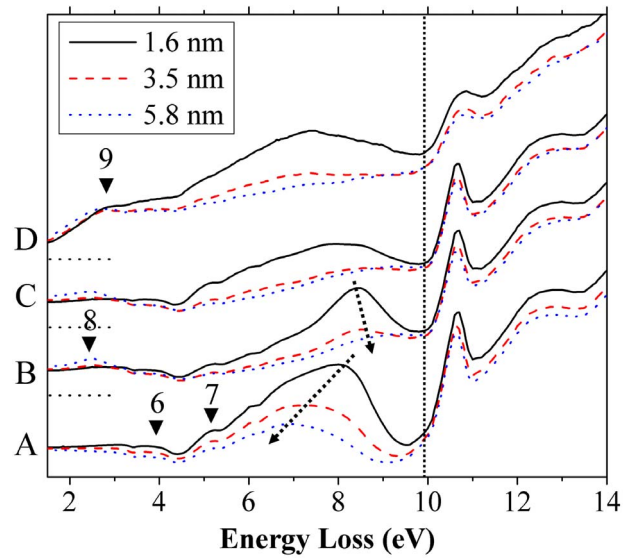


FIG. 5. (Color online) Spectra in SiO₂ for *x*₀=1.6, 3.5, and 5.8 nm, taken with respect to the Si/SiO₂ interface. D, experimental results; A–C, simulations for various configurations (see text). The vertical dotted line indicates the SiO₂ band gap energy.

Experimental spectra displayed at the top of Figs. 4(c) and 4(d) were acquired at two different impact parameters in the HfO₂ layer: one closer to the interface with SiO₂ and the other closer to the interface with TiN. The corresponding modeled spectra are displayed underneath. As the electron probe approaches the TiN layer, the intensity of the 2.5 eV IP increases. Such a variation is also observed around the HfO₂ bulk plasmon energy (arrow 5). In that case, the general decrease of the bulk plasmon intensity near an interface (the Begrenzung effect) is partially compensated by the presence of a second HfO₂/TiN IP at 15.6 eV. This is clearly ascertained by our simulations, where every contributions (bulk, surface Begrenzung) can be isolated. Furthermore, as predicted by the model and also observed in the experiment, delocalization effects remain non-negligible even in the energy range of the semicore Hf O_{2,3} edges.

In order to further investigate the long-range effects due the presence of several parallel interfaces, let us consider the spatially dependent response when the incident probe travels through the neighboring layer of SiO₂. The results (D in Fig. 5) highlight the presence of strong contributions below the SiO₂ band gap energy (9.9 eV, vertical dotted line). Simulated spectra for a single Si/SiO₂ interface (curves A) display a strong IP around 8 eV. As previously explained,⁶ the redshift of the main IP for increasing *x*₀, indicated by the dotted arrow, is attributed to relativistic effects. In contrast, when all layers and interfaces in the stack are accounted for in the simulation (curves B), a slight blueshift of the IP peak is observed. A complete description of the experimental spectra requires in this case to account for interdiffusion and roughness at the boundaries, in particular, for the Si/SiO₂ interface. In our previous study,⁶ this had been modeled by adding an extra 1 nm layer of SiO. In the present analysis, we follow Ref. 20 and insert five extra layers (total thickness of 1 nm) with dielectric constants varying gradually between

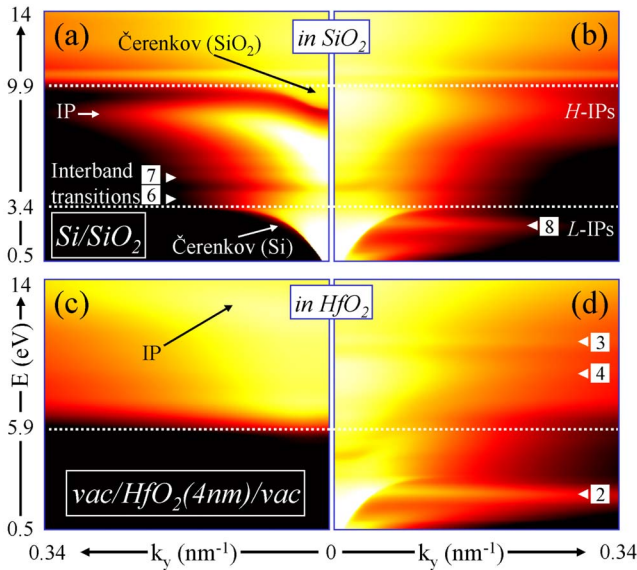


FIG. 6. (Color online) Simulated E - k_y loss images when the probe is at $x_0=5.8$ nm in SiO_2 (top) and at the center of the HfO_2 layer (bottom). The systems consist of (a) Si/SiO_2 , (b) all layers, (c) vacuum/ HfO_2 (4 nm)/vacuum, and (d) all layers. The energy (vertical axis) extends from 0.5 to 14 eV, and k_y (horizontal axis) extends from 0 to 0.34 nm^{-1} (corresponding to $200 \mu\text{rad}$). The intensity is plotted on a logarithmic scale. The numbered arrows refer to the ones in Figs. 4 and 5.

the materials on both side of the interface. Introducing extra layers at each interface in the multilayer system generates spectra C in Fig. 5, which reproduce remarkably well the experimental spectra (D). A possible explanation for the difference in the maximum position of the main IP is the contributions from modes confined near the junctions of the Si/SiO_2 interface and the two vacuum/specimen surfaces running perpendicular.³⁰

To interpret the various spectral features, Fig. 6 presents four simulated loss images, displaying the loss probability as a function of the energy and scattering vector along the y axis (k_y). Scattering angles considered are small compared to the EELS aperture, but include the most intense region. Looking first at an isolated Si/SiO_2 interface when the probe is located in SiO_2 [Fig. 6(a)], the strong IP around 8 eV is shown to disperse as a function of k_y . Interband transitions associated with SiO_2 are visible above the gap (9.9 eV, dotted line), but transitions in Si are also present. The latter are identified by arrows 6 and 7, which correspond to the same arrows in Fig. 5. Below the 9.9 eV gap, a small contribution from Čerenkov radiation in SiO_2 is observed. The emission of Čerenkov photons will occur when electrons travel through a medium with a velocity larger than the speed of light in that medium.^{31,32} In addition, Čerenkov losses are also predicted below the Si direct gap (3.4 eV, dotted line), extending even below the Si indirect gap (1.1 eV). It gives rise to the plateau below 3 eV in the simulated spectra. The origin of the losses in this case is from Čerenkov radiation in Si induced by fast electrons traveling in SiO_2 . Furthermore, because of total internal reflections at the Si/vacuum inter-

faces, this emitted radiation should be interpreted in terms of guided modes,³¹ which are expected to have a low frequency cutoff dependent on the specimen thickness.³² This point explains the drop in signal observed in experimental spectra (arrow 9 in Fig. 5). Such a drop has previously been observed for fast electrons traveling through specimens of different thicknesses.³³

When the probe is located at the same distance from the Si/SiO_2 interface, but for a system where all the layers in the stack have been included, the loss image [Fig. 6(b)] differs considerably. IP coupling (labeled H -IPs) blurs the otherwise well defined Si/SiO_2 plasmon dispersion. This has the effect of moving the IP peak to higher energy loss and inverting the shift as a function of the impact parameter. Additional contributions below 3.4 eV (L -IPs) appear as two well defined branches and produce a peak in the spectra over the Čerenkov plateau (arrow 8 in Fig. 5). L -IPs can be loosely interpreted as coupling between the HfO_2/TiN and the TiN/Si IPs.

Comparing E - k_y maps for an electron traveling in the HfO_2 [Fig. 6(d)] and in the SiO_2 [Fig. 6(b)] layers, it is hardly possible to differentiate based on the features at low angles and energies. A recent study¹ on surface plasmon mapping with EELS offers an explanation. A probe located in SiO_2 or in HfO_2 will excite, in both cases, eigenmodes extending over the whole nanostructure. In contrast to Ref. 1, we note that the eigenmodes are not purely plasmonic, but involve interband transitions and radiative modes. L -IPs appearing in Fig. 6(d) explain the peak below the gap in Fig. 4 (arrow 2). As for the shape of the spectra above the gap onset [Fig. 4(b)], the interband transition in SiO_2 explains the peak indicated by arrow 3, while the coupled H -IPs produce the increase in intensity indicated by arrow 4. Figure 6(d) also highlights excitations at energies close to the HfO_2 band gap (dotted line). This contrasts with the case of a HfO_2 layer embedded in vacuum [Fig. 6(c)], where no losses occur below the gap onset.

IV. CONCLUSION

In summary, although spatially resolved EELS measurements have been successful in extracting gap values for bulk specimens³⁴ and freestanding nanostructures,² such methods cannot be directly applied to layer systems incorporating thin dielectrics. Delocalized contributions associated with interface plasmons, interband transitions, and Čerenkov radiation may overlap with the local band structure information. These modes may originate not only from boundary conditions with the probed layer but also from a coupling between all interface modes within the system. The comparison between experiments and simulations points to noticeable similarities in character between bulk HfO_2 and the layer material. Some states in the gap of the HfO_2 material of the thin layer, with no equivalent in the bulk, may exist, but we are here close to the noise induced detection limit. A successful extraction of such contributions would depend on the precision of the model we have discussed, including the details of the structural representation of interfacial regions and a careful

consideration of the probe propagation. The present results nevertheless demonstrate that a relativistic description for the interaction of the incoming electrons with the whole layered structure provides a basis for interpretation and is necessary to identify and disentangle the various loss signals.

ACKNOWLEDGMENTS

We would like to thank Brendan Foran of ATDF-

SEMATECH for providing the subject sample. The authors are grateful to Mike Walls and Marcel Tencé for assistance and to Adrien Dousse for preliminary work. This work has been partly funded by the I3 European project ESTEEM under Contract No. 026019. M.C. acknowledges financial support from the Education Office (Chateaubriand committee) of the Embassy of France in Canada and the Natural Sciences and Engineering Research Council of Canada.

*Present address: Department of Applied and Engineering Physics, Cornell University; m.couillard@cornell.edu

- ¹J. Nelayah, M. Kociak, O. Stéphan, M. Tencé, L. Henrard, D. Taverna, I. Pastoriza-Santos, L. M. Liz-Marzà, and C. Colliex, *Nat. Phys.* **3**, 348 (2007).
- ²R. Arenal, O. Stéphan, M. Kociak, D. Taverna, A. Loiseau, and C. Colliex, *Phys. Rev. Lett.* **95**, 127601 (2005).
- ³O. Stéphan, D. Taverna, M. Kociak, K. Suenaga, L. Henrard, and C. Colliex, *Phys. Rev. B* **66**, 155422 (2002).
- ⁴M. Kociak, O. Stéphan, L. Henrard, V. Charbois, A. Rothschild, R. Tenne, and C. Colliex, *Phys. Rev. Lett.* **87**, 075501 (2001).
- ⁵L. D. Marks, *Solid State Commun.* **43**, 727 (1982).
- ⁶P. Moreau, N. Brun, C. A. Walsh, C. Colliex, and A. Howie, *Phys. Rev. B* **56**, 6774 (1997).
- ⁷A. Howie and R. H. Milne, *Ultramicroscopy* **18**, 427 (1985).
- ⁸K. van Benthem, G. L. Tan, L. K. DeNoyer, R. H. French, and M. Ruhle, *Phys. Rev. Lett.* **93**, 227201 (2004).
- ⁹A. Gutiérrez-Sosa, U. Bangert, A. J. Harvey, C. J. Fall, R. Jones, P. R. Briddon, and M. I. Heggie, *Phys. Rev. B* **66**, 035302 (2002).
- ¹⁰P. E. Batson, K. L. Kavanagh, J. M. Woodall, and J. W. Mayer, *Phys. Rev. Lett.* **57**, 2729 (1986).
- ¹¹J. Robertson, *Rep. Prog. Phys.* **69**, 327 (2006).
- ¹²M. P. Agustin, G. Bersuker, B. Foran, L. A. Boatner, and S. Stemmer, *J. Appl. Phys.* **100**, 024103 (2006).
- ¹³B. Foran, J. Barnett, P. S. Lysaght, M. P. Agustin, and S. Stemmer, *J. Electron Spectrosc. Relat. Phenom.* **143**, 149 (2005).
- ¹⁴A. J. Craven, M. MacKenzie, D. W. McComb, and F. T. Docherty, *Microelectron. Eng.* **80**, 90 (2005).
- ¹⁵M. Couillard, M.-S. Lee, D. Landheer, X. Wu, and G. A. Botton, *J. Electrochem. Soc.* **152**, F101 (2005).
- ¹⁶G. D. Wilk and D. A. Muller, *Appl. Phys. Lett.* **83**, 3984 (2003).
- ¹⁷M. C. Cheynet, S. Pokrant, F. D. Tichelaar, and J.-L. Rouvière, *J. Appl. Phys.* **101**, 054101 (2007).
- ¹⁸M. P. Agustin, L. R. C. Fonseca, J. C. Hooker, and S. Stemmer, *Appl. Phys. Lett.* **87**, 121909 (2005).
- ¹⁹H. Raether, *Excitations of Plasmons and Interband Transitions by Electrons* (Academic, London, 1980).
- ²⁰J. P. R. Bolton and M. Chen, *J. Phys.: Condens. Matter* **7**, 3373 (1995); **7**, 3389 (1995).
- ²¹The code can be obtained by contacting the authors.
- ²²C. Jeanguillaume and C. Colliex, *Ultramicroscopy* **28**, 252 (1989).
- ²³R. F. Egerton, *Electron Energy-loss Spectroscopy in the Electron Microscope* (Plenum, New York, 1996).
- ²⁴A. Gloter, A. Douiri, M. Tencé, and C. Colliex, *Ultramicroscopy* **96**, 385 (2003).
- ²⁵E. D. Palik, *Handbook of Optical Constants* (Academic, Orlando, 1998).
- ²⁶A. N. Saxena and K. L. Mittal, *J. Appl. Phys.* **46**, 2788 (1975).
- ²⁷L. K. Dash, N. Vast, P. Baranek, M.-C. Cheynet, and L. Reining, *Phys. Rev. B* **70**, 245116 (2004).
- ²⁸P. M. Echenique, *Philos. Mag. B* **52**, L9 (1985).
- ²⁹T. Neyer, P. Schattschneider, J. P. R. Bolton, and G. A. Botton, *J. Microsc.* **187**, 184 (1997).
- ³⁰J. Aizpurua, A. Howie, and F. J. García de Abajo, *Phys. Rev. B* **60**, 11149 (1999).
- ³¹F. J. García de Abajo, A. Rivacoba, N. Zabala, and N. Yamamoto, *Phys. Rev. B* **69**, 155420 (2004).
- ³²J. D. Jackson, *Classical Electrodynamics* (Wiley, New York, 1999).
- ³³M. Stoger-Pollach, H. Franco, P. Schattschneider, S. Lazar, B. Schaffer, W. Grogger, and H. W. Zandbergen, *Micron* **37**, 396 (2006).
- ³⁴B. Rafferty and L. M. Brown, *Phys. Rev. B* **58**, 10326 (1998).